FISEVIER

#### Contents lists available at ScienceDirect

### Microporous and Mesoporous Materials

journal homepage: www.elsevier.com/locate/micromeso



# Understanding the role of Zn<sup>2+</sup> in surfactant-free layered silicate delamination: Exfoliation of magadiite



Alexander Okrut<sup>a</sup>, Nicolás A. Grosso-Giordano<sup>a</sup>, Christian Schöttle<sup>a</sup>, Stacey Zones<sup>b,\*</sup>, Alexander Katz<sup>a,\*\*</sup>

- <sup>a</sup> Department of Chemical and Biomolecular Engineering, University of California at Berkeley, Berkeley, CA, 94720, USA
- b Chevron Energy Technology Company, Richmond, CA, 94801, USA

#### ARTICLE INFO

#### Keywords: Magadiite Delamination mechanism Exfoliation Zinc-oxide nanoparticles

#### ABSTRACT

We investigated the effect of  $Zn^{2+}$  treatment on the exfoliation of layered silicate magadiite, as a model system, to better understand the role of zinc in surfactant-free zeolite exfoliation. Samples of magadiite and ball-milled magadiite were exfoliated via treatment with aqueous  $Zn(NO_3)_2$  solution, and the resulting materials were characterized via powder X-ray diffraction, nitrogen physisorption, high-angle annular dark-field scanning transmission electron microscopy, and infrared spectroscopy.  $Zn^{2+}$  treatment of magadiite increases its external surface area by 40%, while  $Zn^{2+}$  treatment of ball-milled magadiite increases its external surface area by 109%. Acid-washing removes  $Zn(O)_x(OH)_y$  colloids and further increases external surface area, leading to a total surface area increase of 150% for magadiite after  $Zn^{2+}$  treatment and acid-washing, and 182% for ball-milled magadiite after  $Zn^{2+}$  treatment due to pore blocking. We propose a mechanism of exfoliation to account for these surface-area increases, which involves the  $Zn(O)_x(OH)_y$  colloids growing and forcing layers apart selectively at the grain boundaries. Ball milling not only makes existing grain boundaries more accessible, but it also creates new grain boundaries, resulting in more efficient exfoliation.

## 1. We are pleased to be making a contribution in honor of professor Roth for this special issue which honors him

Dr. Roth is well-known through the patent literature initially. The laboratories of Mobil in New Jersey, USA were the world leaders in zeolite discovery and conversion to commercial applications when Dr. Roth was there. Some key areas which we followed with keen interest were the development of mesoporous materials through the use of surfactant molecule as capable of bringing local order to silicates. This was a totally unforeseen discovery and launched a very vigorous research activity around the world. The materials in themselves, as developed by Mobil, and later other groups, allowed for whole new possibilities in separations and catalysis, capturing a molecular range in between zeolites and amorphous materials. To date, these materials continue to be used and developed, more than 20 years later. For his contributions in this area Dr. Roth was part of the team given the Breck Award by the International Zeolite Association, its highest honor.

Additionally, Dr. Roth also became one of the world's experts on a very interesting and important class of zeolite materials. These were the

materials created around the MWW structure, which workers at Mobil came to recognize as a complex 3-dimensional structure which crystallizes with repeated layered segments. These segments could be expanded, swelled and pulled apart to create a variety of catalysts with important novel features [1,2]. One of the unexpected outcomes was the creation of shape-selective sites for catalysis which nonetheless lie on an external surface of a material. This provides the best of both worlds in that one now has catalytic selectivity and much improved diffusivity. Dr. Roth in recent years, along with Mobil colleague Douglas Dorset, published the most important (and widely used) review in describing the various types of zeolites which have been found which exhibit this structure conversion opportunity [3,4].

Most recently Dr. Roth has been part of the team of Professor Cejka and Morris in developing some very exciting new zeolite chemistry. This would be the chemistry described as "Assembly- Disassembly-Reassemble-Organization" (termed "ADOR"), where certain zeolite structures provide the opportunity to be "disassembled" using chemical methods, and then a variety of techniques were invented as to how to take the components and reconnect them to produce new zeolite

E-mail addresses: aokrut@berkeley.edu (A. Okrut), sizo@chevron.com (S. Zones), askatz@berkeley.edu (A. Katz).

<sup>\*</sup> Corresponding author.

<sup>\*\*</sup> Corresponding author

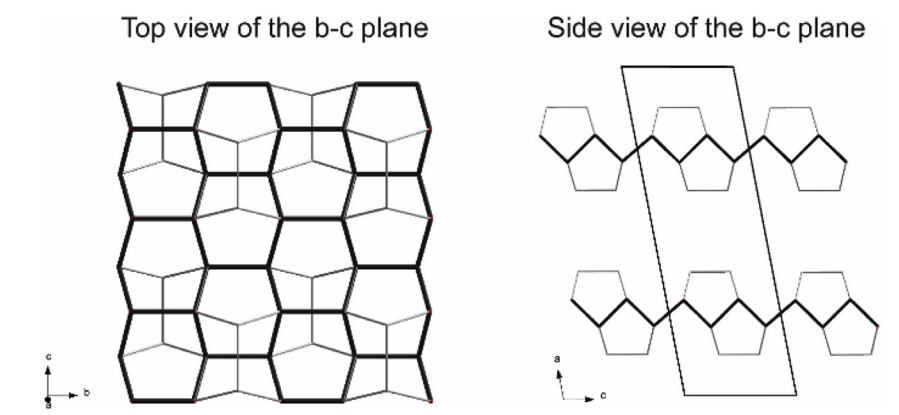


Fig. 1. Model structure of magadiite. The sheets of 6-member rings along the b-c plane are highlighted using dark bold bonds. The 5-membered rings can be seen in the side views of the b-c plane.

structures never seen before. So here one has a totally new methodology for creating new zeolite structures. Along with the invention of new structures comes the opportunity for brand new zeolites to find commercial niches for the benefit of process applications. Indeed, we would say an important part of the recent zeolite technology has been to find new materials which excel in the catalysis for managing waste and potential pollutants which come with industrial activities; this is certainly one of our great new frontiers and challenges [5.6].

If one looks over this suite of technological advances that we have mentioned in the field of zeolite materials and catalysis, it is interesting to note that Dr. Roth appears to be where the breakthroughs occur! This tells one about his keen observations on experimental materials and what could be created next. It also is representative of his depth in materials synthesis, then characterization, and finally applications. His involvement has led to a number of commercial realizations from the discoveries made.

#### 2. Introduction

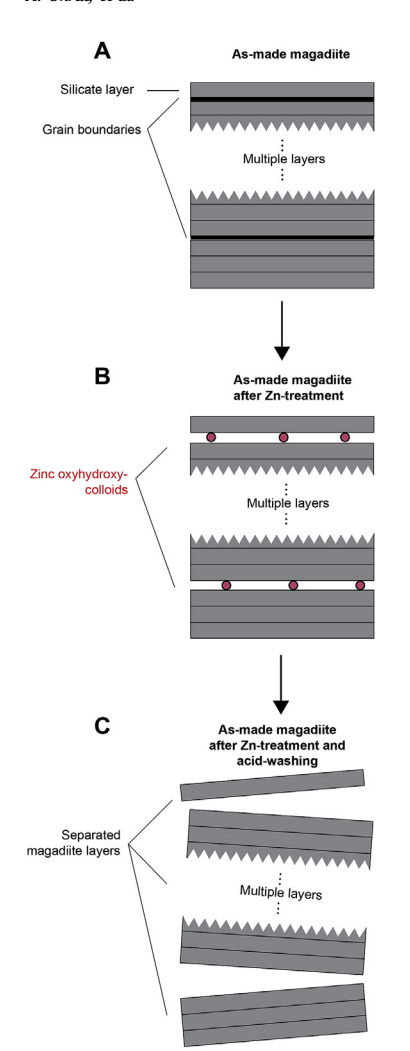
A practical approach for increasing accessible surface area of layered functional materials, including graphene [7], clay [8], and layered zeolite precursors [9-12], is to delaminate these layers, thereby producing a house-of-cards assembly of thin sheets arranged in a disordered fashion [9,11,13-18]. While strictly speaking delamination (having its root in clay materials) is the taking apart of a layered precursor into individual single layers, within the context of zeolites [19], where delamination is always observed with exfoliation (i.e. thin stacks of several layers - not single sheets), delamination of zeolites typically refers to increasing the external surface area of zeolite catalysts by a combination of delamination and exfoliation, a definition we adhere to here. This enables the conversion of bulky substrates that are otherwise unable to access catalytic sites within zeolitic micropores [20]. Zeolite delamination is a complementary method to other approaches such as synthesis of small colloidal zeolite particles [21-23], multilamellar materials [24], extra-large pore zeolites [25,26], single-unit cell zeolite nanosheets [27–29], hierarchically nano-porous zeolite-like materials [30,31], and self-pillared zeolite nanosheets [32]. While a variety of methods exist for zeolite delamination, nearly all of them rely on organic surfactants and sonication, both of which are expensive; in particular sonication is difficult to scale up in a cost-effective manner.

Recently, three notable reports described the synthesis of high external-surface area zeolites via surfactant- and sonication-free approaches that rely on  $Zn(NO_3)_2$  [33,34]. Inayat et al. successfully synthesized layer-like Faujasite zeolite during hydrothermal synthesis in the presence of  $Zn(NO_3)_2$  (Si:Zn=11.4 in the zeolite-synthesis gel), which led to a decreased micropore volume compared to a conventional Faujasite control sample [34]. Separately, Ouyang et al. reported the delamination of MWW-based borosilicate layered zeolite precursor

ERB-1(P) after treatment with  $Zn(NO_3)_2$  [33], resulting in external-surface-area-increases of a factor of ~2.5, without damaging the intralayer order. The delaminated ERB-1, named DZ-1, was also deboronated by zinc treatment, allowing the insertion of a series of Lewis-acid heteroatoms into framework vacancies previously occupied by boron. These reinserted heteroatoms, such as  $Ti^{4+}$  and  $Sn^{4+}$ , were found to be isolated framework cations that were catalytically active for the Baeyer-Villiger oxidation reaction [35]. Recently, Okrut et al. reported the surfactant- and sonication-free delamination of zeolite precursor B-SSZ-70(P) using  $Zn(NO_3)_2$  in combination with tetrabutylammonium fluoride, which yields delaminated zeolite DZ-2 [10]. Like its predecessor DZ-1, DZ-2 allows the insertion of Lewis-acid heteroatoms into its framework, with Ti-DZ-2 being a highly active, selective, and stable olefin epoxidation catalyst when using organic hydroperoxides as oxidants [10].

The goal of this manuscript is to shed further light on the role of zinc in the delamination of a layered precursor material, such as B-SSZ-70(P) and ERB-1(P), from the perspective of such materials being noncovalent assemblies of building blocks, i.e., zeolite sheets that are not covalently crosslinked in the precursor materials and instead are terminated by SiO Na + or SiO (organic cation) + functionality between the zeolite sheets [36]. We use crystalline layered silicate magadiite as a simple yet relevant model of a more complex layered zeolite precursor material such as crystalline borosilicate B-SSZ-70(P) and ERB-1(P). Magadiite is a sodium silicate mineral with a layered structure consisting of negatively charged silicate layers and balancing sodium cations between the layers, which are separated by an interlayer spacing of 13.5 Å [37]. Fig. 1 shows a model of the magadiite structure, which consists of layers of 6-membered rings in the boat conformation, pairs of which are capped with siloxane functionality that resemble an "A" frame both above and below the 6-membered ring sheets. Atop the "A" frame capping groups are silanol Q3 sites - the only silanols present in magadiite, resulting in a Q<sup>4</sup>/Q<sup>3</sup> ratio of 2 [37]. Surfactants have been successfully intercalated between layers in magadiite, including those based on CTAB and alkylpyridinium [38,39]. It has also been delaminated at high pH using TPAOH to synthesize a material that was judged to be up to 60% delaminated [40,41], however, to the best of our knowledge, magadiite has not been previously delaminated under mild conditions of near-neutral pH, as we perform here.

Based on prior reports of an interface formed between zinc oxide nanoparticles and magadiite layers [42], we formulated a hypothesis on how  $\mathrm{Zn}^{2+}$  could play a role in magadiite delamination under nearneutral conditions, which is shown in Fig. 2. Our hypothesis involves the formation of an interface between  $\mathrm{Zn}(O)_x(OH)_y$  colloidal particles and magadiite specifically at grain boundaries, as those regions of the layered material are the most accessible for  $\mathrm{Zn}(O)_x(OH)_y$  colloidal particles to easily intercalate into. Such grain boundaries have been previously demonstrated to be general occurrences also within zeolite



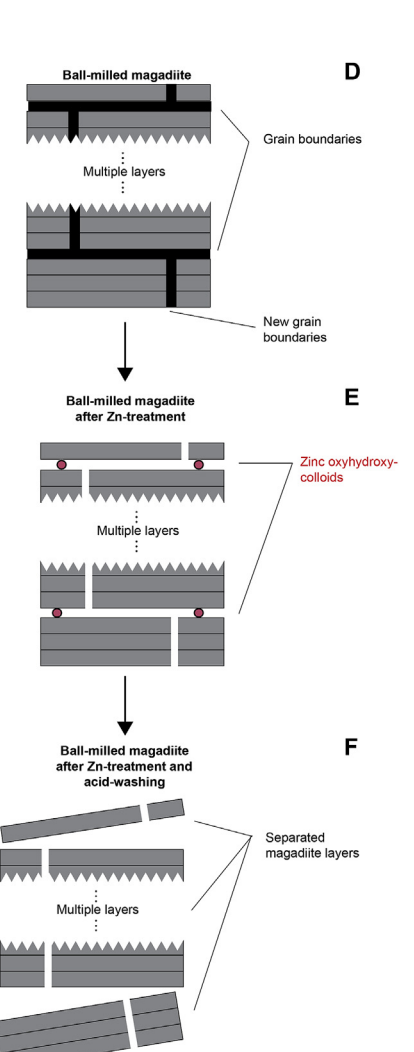


Fig. 2. Schematic representation of the proposed effect of Zn2+ treatment followed by acid-washing on magadiite (a-c) and ball-milled magadiite (d-f). (a) Layered silicate magadiite possesses narrow grain boundaries, preferably between layers. (b) Zn (O)<sub>x</sub>(OH)<sub>v</sub> colloids grow at the silicate surface at the grain boundaries upon Zn(NO<sub>3</sub>)<sub>2</sub> treatment and force magadiite layers apart. The same Zn(O)<sub>x</sub>(OH)<sub>v</sub> colloids block the pores that are formed through layer separation. (c) Upon acid-washing, the Zn particles are removed and liberated external surface area is exposed. (d) Ball-milling of magadiite opens existing grain boundaries and creates new ones. (e) Zntreatment of ball-milled Magadiite leads to layer separation. The resulting external surface area is immediately accessible via new grain boundaries. (f) Upon acid-washing, only little additional surface area becomes exposed.

particles, where they have been invoked to play an important role in catalysis and have been elegantly characterized by electron tomography [43]. In addition, studies involving metal nanoparticles nucleated and grown in zeolites can demonstrate discrete lines observable by STEM and TEM microscopy of the formed metal nanoparticles. Such lines could be consistent with grain boundaries acting as preferential nucleation sites [44,45]. Our hypothesis further involves a growing Zn  $(O)_x(OH)_y$  colloidal particle at this interface acting as the equivalent of a mechanical nanoscale wedge, presumably driven by the repulsion of charge at the surface of the  $Zn(O)_x(OH)_y$  colloids [46], which forces adjacent layers apart as these colloids grow, as represented schematically on the left side of Fig. 2.

The goal of this manuscript is to investigate whether there is experimental evidence to support the mechanism of delamination schematically depicted in Fig. 2, i.e. formation and growth of  $\text{Zn}(O)_x(OH)_y$  colloids within grain boundaries of the magadiite silicate when treating layered magadiite with  $\text{Zn}(NO_3)_2$  in aqueous solution. Our motivation in investigating this for the particular case of magadiite is that, if plausible, such a mechanism could also apply to the delamination of other crystalline layered inorganic-oxide materials. To test the role of grain boundaries as nucleation sites for  $\text{Zn}(O)_x(OH)_y$  colloidal particle growth, we designed a comparative analysis of magadiite delamination with and without prior ball milling. The ball milling serves as a perturbation that is envisioned to (i) make existing grain boundaries in magadiite more accessible while also (ii) possibly creating new ones, as represented in Fig. 2. Thus, our approach is to compare  $\text{Zn}^{2+}$ -promoted magadiite delamination in the ball-milled material with the same

material except in the absence of ball milling. If grain boundaries play a significant role, then the greater accessibility of grain boundaries in ball-milled magadiite should result in a more open structure after zinc treatment relative to a material treated with  $\mathrm{Zn^{2+}}$  without ball milling. In addition, we expect to observe a greater degree of delamination and surface area enhancement after zinc removal, in the final delaminated material, for the magadiite that underwent prior ball milling before zinc treatment. The extent of delamination at crucial junctures along the delamination path is characterized via measurement of the BET and external surface area of magadiite, TEM (transmission electron microscopy) and HAADF-STEM (high-angle annular dark-field scanning transmission electron microscopy). We also used FTIR (Fourier transform infrared) spectroscopy and H-D isotopic exchange of silanols in magadiite to probe for pore blocking at intermediate stages, prior to Zn  $(O)_x(OH)_y$  colloid removal via acid treatment.

#### 3. Experimental

Magadiite was synthesized as described in literature [39]:  $1.23\,g$  NaOH were dissolved in 30 mL water and mixed with  $18.5\,g$  of colloidal silica in water (40 wt % silica). The mixture was transferred into  $50\,m$ L Teflon liners and heated in an autoclave at  $150\,^{\circ}$ C for 8 days. Powder X-ray diffraction (XRD) on a Siemens D5000 diffractometer confirmed the formation of magadiite. Our Zn treatment protocol of magadiite follows that of Ozawa et al. [42]:  $20\,m$ L of a  $0.5\,M$  Zn(NO<sub>3</sub>)<sub>2</sub> solution was added to  $0.6\,g$  of magadiite, and the mixture was stirred for  $48\,h$  at  $25\,^{\circ}$ C, followed by filtration and washing with water. A separate sample

of magadiite was ball-milled at 300 rpm for 20 min using a planetary mill type Pulverisette 5/4 by FRITSCH, prior to Zn<sup>2+</sup> treatment. Following Zn<sup>2+</sup> treatment, selected samples were acid washed by stirring 200 mg of sample in 10 mL of a 2 M aqueous HNO3 solution at 135 °C for 16 h. Samples for nitrogen physisorption were calcined at 350 °C for 12 h (sufficient to remove surface-bound water) and measured on an ASAP 2020 apparatus by Micromeritics. Transmission electron microscopy (TEM) and high-angle annular dark-field scanning transmission electron microscopy (HAADF-STEM) were performed on a FEI Tecnai F20 operated at 200 kV. Samples suitable for TEM and HAADF-STEM were prepared on Lacey carbon on copper grids. Transmission Fouriertransform infrared spectra were acquired for self-supported wafers in an in-situ flow cell (In-situ Research Instruments, Inc., South Bend, IN), while the pellet remained under He flow (50 mL min<sup>-1</sup>) and heated to 200 °C; materials were treated in-situ with gas-phase D2O by addition of 0.1 mL of D2O through a septum into the heated He flow lines, followed by purging in pure He.

#### 4. Results and discussion

## 4.1. Characterization of magadiite and the effect of its treatment with Zn $(NO_3)_2$

The structure of magadiite was characterized via powder X-ray diffraction (PXRD), and this data is shown in Fig. 3. Based on published data [37], all of the observed peaks in the XRD pattern are assignable to sodium magadiite. Nitrogen physisorption data of the calcined magadiite demonstrate a lack of uptake at low pressures (below P/P<sub>0</sub> of 0.2),

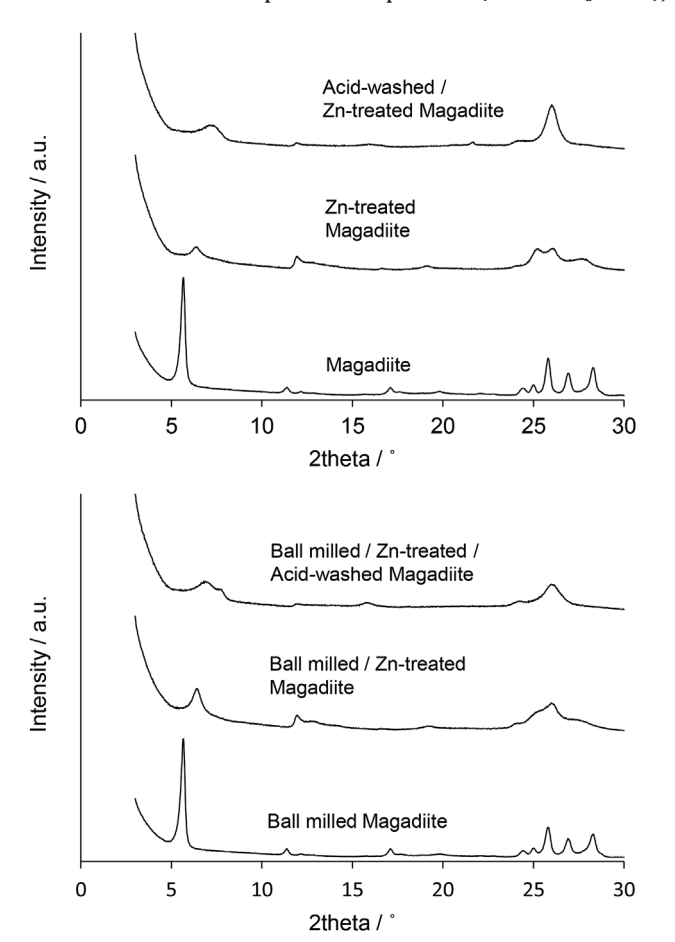


**Fig. 3.** Powder XRD pattern of the materials indicated above each pattern. Sharp peaks indicate that magadiite is crystalline and that ball milling of magadiite has no effect on its crystallinity. Zn treatment leads to a decrease of peak intensity for both magadiite and the ball-milled magadiite.

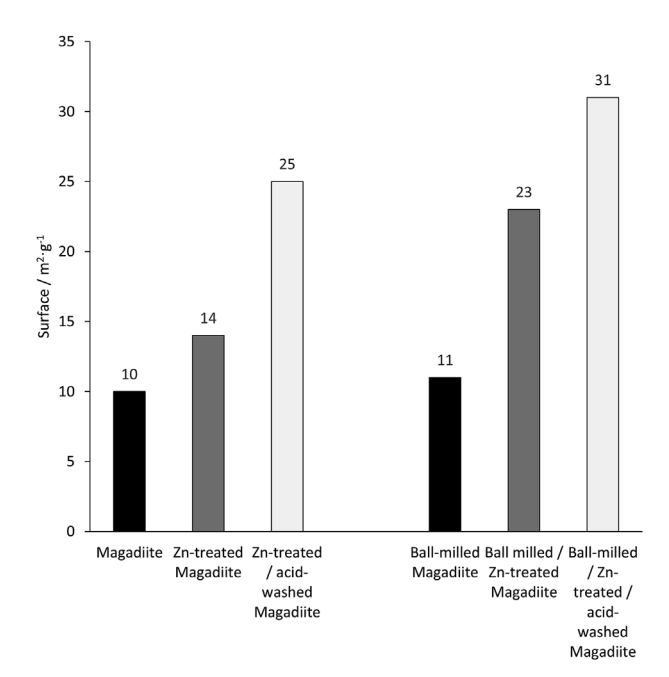


Fig. 4. External surface area of magadiite materials before and after various treatments

suggesting a lack of micropores in calcined magadiite (Figs. S1 of Supplementary Information and S2). This is supported by a micropore volume of this material of nearly zero, as calculated with the t-plot method (Table 1). Calcined magadiite has an external surface area of  $10\,\mathrm{m}^2/\mathrm{g}$ . HAADF-STEM and TEM images of magadiite in Fig. 5 reveal the layered nature of this material, showing highly symmetrical stacked sheets along the z-axis, which are in the micrometer range. These sheets are arranged in a parallel fashion and packed densely, allowing little pore space between layers, beyond that nominal distance required for non-covalent interaction between sheets.

We treated magadiite in a 0.5 M aqueous Zn(NO<sub>3</sub>)<sub>2</sub> solution for 48 h at 25 °C, conditions that facilitate the formation of zinc-containing colloidal species on the magadiite surface, which upon heating forms ZnO nanoparticles [42]. We characterized the resulting material by elemental analysis, nitrogen physisorption, powder X-ray diffraction, TEM, HAADF-STEM, and FTIR spectroscopy. Upon addition of magadiite to a  $0.5\,\mathrm{M}$  aqueous  $\mathrm{Zn}(\mathrm{NO_3})_2$  solution, the pH of the solution increased immediately from 4.5 to 5.3 and subsequently decreased to 4.7 within 1 h. Within 48 h, the pH slightly dropped to 4.3. Data from TEM and HAADF-STEM images in Fig. 5 show the layered structure of magadiite intact after Zn2+ treatment, with a small fraction of layers separated and the aforementioned colloids on the external magadiite surface, observable as dark spots. Experiments to identify the chemical composition of the colloids via FTIR spectroscopy show that these colloids do not comprise  $Zn_{(x+y)/2}(OH)_x(NO_3)_y$ , because the strong characteristic nitrate band at 1350 cm<sup>-1</sup> is absent in our material (see inset in Fig. 6c and Fig. S7, Supporting Information) [47]. Knowing that these colloids form ZnO particles upon heating [42], we invoke the formation of Zn(O)x(OH)v colloids and explain the stability of the precipitated Zn(O)x(OH)v particles at pH 4.3 to be a consequence of their reduced solubility in confined spaces of grain boundaries, a general effect that has been previously observed [48,49]. The external surface area of Zn-treated magadiite was measured to be 14 m<sup>2</sup>/g, which corresponds to a 40% increase, relative to the calcined magadiite without Zn(NO<sub>3</sub>)<sub>2</sub> treatment. PXRD data in Fig. 3 show that the peak at 5.67° shifted to 6.38° and became broader and lower in intensity upon Zn(NO<sub>3</sub>)<sub>2</sub> treatment, indicating loss of long-range order along the direction perpendicular to the stacking of the layers. The observed decrease in the d-spacing is presumably a consequence of a single Zn<sup>2+</sup>

 $\begin{tabular}{ll} \textbf{Table 1} \\ \textbf{Summary of textural properties and Na/Zn content for various samples}. \\ \end{tabular}$ 

Material	BET surface area (m <sup>2</sup> /g)	External surface area (m <sup>2</sup> /g)	Micropore Volume (mL/g)	Na-content (wt%)	Zn-content (wt%)
As-made magadiite	16	10	< 0.01	4.15	0
Zn treated magadiite	33	14	0.01	< 0.02	5.99
Ball-milled magadiite	21	11	0.01	4.15	0
Ball-milled/Zn-treated magadiite	42	23	0.01	N/A	4.72

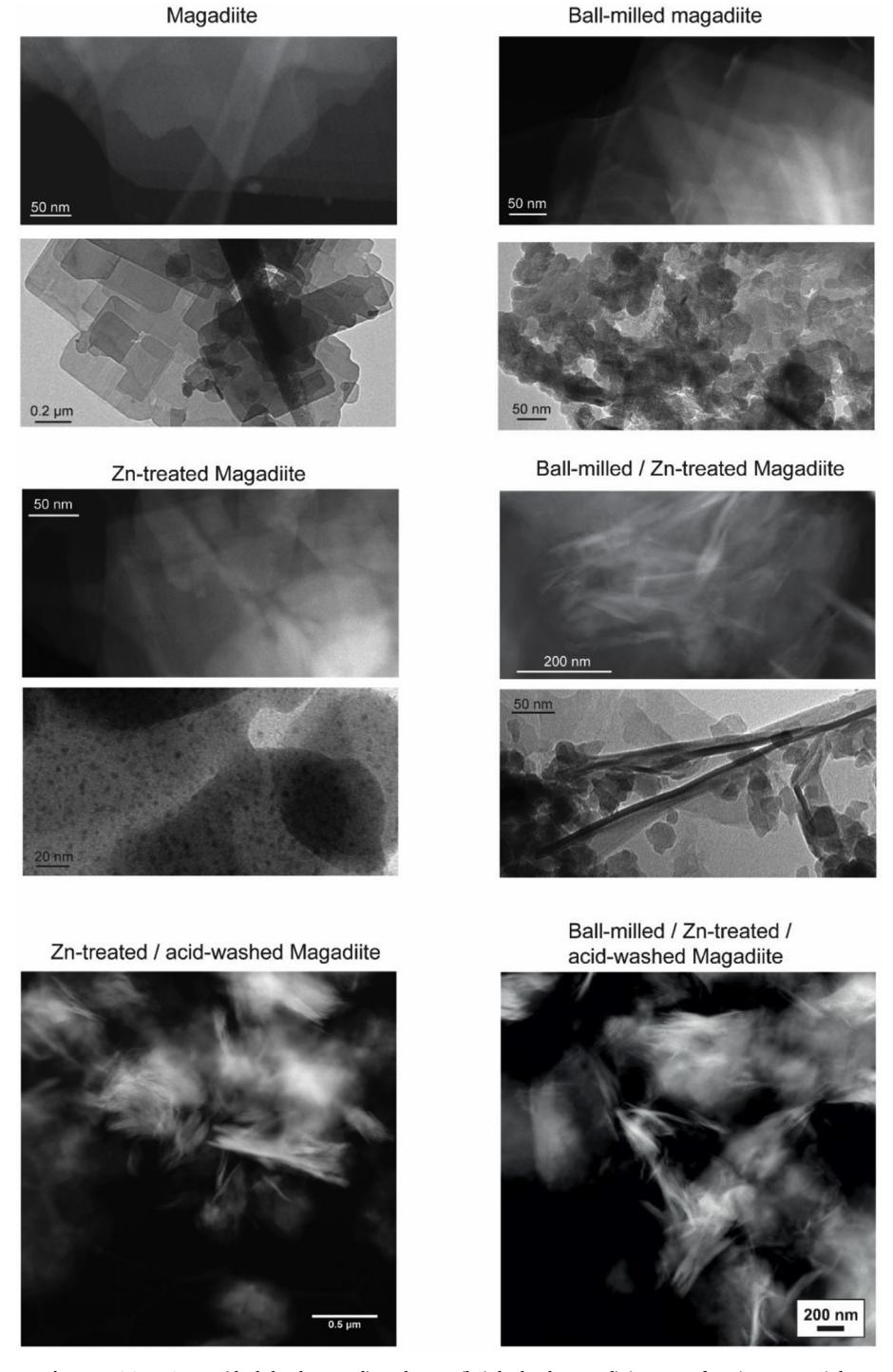
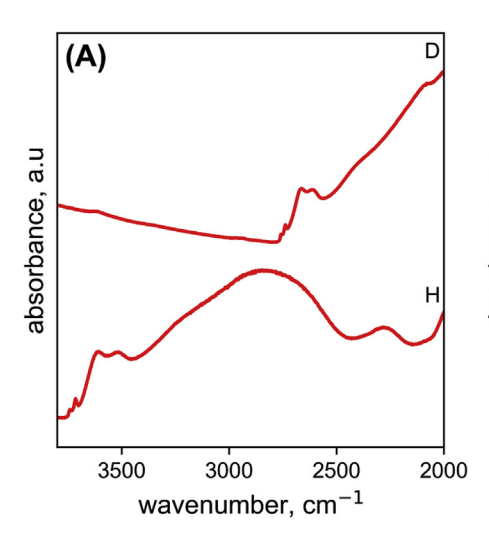
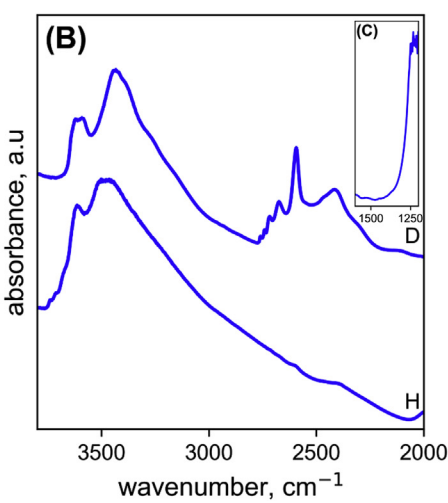


Fig. 5. HAADF-STEM (dark background) and TEM (bright background) images of various materials.





**Fig. 6.** Transmission Fourier-transform infrared spectra for (A) magadiite and (B) Zn-treated magadiite. Spectra labelled 'H' correspond to a self-supported wafer of the material under He flow  $(50 \, \text{mL min}^{-1})$  at 473 K; spectra labelled 'D' to the same wafer after treatment with gas-phase  $D_2O$  under He flow at 473 K for 10 min, following purging with pure He for 20 min at 473 K. Inset (C) shows the absence of a  $NO_3$  –band at  $1350 \, \text{cm}^{-1}$  in  $Zn(NO_3)_2$ -treated magadiite and a band attributed to silica in the vicinity of  $1250 \, \text{cm}^{-1}$  [55].

that intercalates between non-delaminated magadiite layers and completely exchanges with two Na+ there, thereby reducing the magadiite interlayer distance. This is supported by elemental analysis and FTIR spectroscopy of magadiite and  ${\rm Zn^{2+}}$ -treated magadiite: While magadiite has a Na-content of 4.2 wt%, virtually none of it remains after Zn<sup>2+</sup>-treatment (0.02 wt% Na), whereas the Zn<sup>2+</sup>-treated magadiite contains 5.99 wt% zinc. Consistent with this, FTIR spectroscopy of magadiite after Zn<sup>2+</sup>-treatment shows the disappearance of its intense, broad feature spanning the region between 3400 cm<sup>-1</sup> and 2500 cm<sup>-1</sup> in Fig. 6b, which has previously been assigned to OH species in interaction with interlayer NaOH (Fig. 6a) [44]. We underscore that while we are indeed growing Zn-containing colloids in grain boundaries (Fig. 2), which would be expected to locally increase interlayer spacing, this effect is not detected via powder X-ray diffraction because of disorder in the areas where the Zn-containing colloids are located and because these areas are a much smaller fraction of the material compared to all of the interlayer regions mentioned above. Because of the mild pH under which Zn treatment occurs, we exclude dissolution and/ or amorphization of the magadiite material as a reason for both the observed peak intensity decrease in the PXRD pattern as well as the observed surface-area increase. We further exclude exchange of Na<sup>+</sup> for H<sup>+</sup>, because the measured pH range from 4.3 to 5.5 is not sufficient for such an exchange (see Supporting Information and Fig. S4). Although the Zn-content of magadiite after aqueous Zn(NO<sub>3</sub>)<sub>2</sub> treatment was measured to be 5.99 wt%, no diffraction peaks for bulk ZnO were observed, which further supports TEM data, which showed the formation of small (< 5 nm) colloids in the form of dark spots on the magadiite surface. Altogether, the data above show that the textural properties of magadiite change upon treatment with Zn(NO<sub>3</sub>)<sub>2</sub>, including an increase in external surface area. A significant amount of Zn remains within this material (5.99 wt%), corresponding to material B in Fig. 2, as a result of both Zn<sup>2+</sup> intercalation as well as nucleation and growth of small Zn (O)<sub>x</sub>(OH)<sub>v</sub> colloids in between magadiite layers.

Upon acid-washing, the surface area of Zn-treated magadiite increases further, to an external surface area of  $25\,\mathrm{m}^2/\mathrm{g}$ , corresponding to a total external surface area increase of 150%, relative to the calcined magadiite without  $\mathrm{Zn}(\mathrm{NO_3})_2$  treatment. This increase in surface area is also reflected in HAADF-STEM images, which show a dramatic change from the mostly intact magadiite layers of the material before acid washing, to delaminated layers after acid-washing, as shown in Fig. 5. These images of the delaminated layers are similar in their open nanoscale morphology to STEM images of delaminated borosilicate zeolites synthesized via  $\mathrm{Zn}^{2+}$  treatment, such as DZ-1 (delaminated ERB-1(P)) and DZ-2 (delaminated B-SSZ-70(P)) [10,33]. According to elemental analysis, virtually all  $\mathrm{Zn}^{2+}$  has been removed from the sample after acid-washing (< 0.02 wt% Zn).

4.2. Characterization of magadiite and the effect of its treatment with Zn  $(NO_3)_2$  by infrared spectroscopy

Magadiite samples before and after treatment with Zn(NO<sub>3</sub>)<sub>2</sub> were studied by FTIR spectroscopy to understand changes to surface structure of the silicate layers with results shown in Fig. 6. The bottom FTIR spectrum in Fig. 6a corresponds to magadiite, heated to 200 °C under a flow of dry helium to remove weakly bound water. Several distinct bands are evident in this spectrum, corresponding to stretching vibrations of different OH species [50]. Stretching vibrations at 3741 cm<sup>-1</sup> coincide with frequencies observed for free isolated silanols on the surface of amorphous silica [51,52]; their relatively weak contribution suggests that they correspond to silanols on the terminating surface of magadiite crystallites, which are a minority species relative to contributions from interlayer OH groups. We therefore assign the band at  $3741\,\mathrm{cm}^{-1}$  to free isolated silanols on the terminating surface of magadiite crystallites. Bands red shifted from these free silanols at 3741 cm<sup>-1</sup>, the first of which is observed at 3717 cm<sup>-1</sup>, correspond to silanols perturbed by H-bonding, by analogy to assignments on amorphous silica [51,52]. Broad and intense features are also observed at 3610 cm<sup>-1</sup> and 3510 cm<sup>-1</sup>, corresponding to other H-bonded silanols species [50]; it should be noted that features in this spectral region may also arise from strongly bound inter-layer water [53], which may not have been fully removed by treatment at 200 °C [50]. An intense, broad feature spanning the region between 3400 cm<sup>-1</sup> and 2500 cm<sup>-1</sup> is also evident and has previously been assigned to OH species in interaction with interlayer NaOH [50].

The bottom infrared spectrum in Fig. 6b corresponds to magadiite after treatment with Zn(NO<sub>3</sub>)<sub>2</sub>, measured at the same conditions as magadiite. The same characteristic OH species that were observed for magadiite are present here, with stretching vibrations at 3741 cm<sup>-1</sup>, 3717 cm<sup>-1</sup>, 3610 cm<sup>-1</sup> and 3510 cm<sup>-1</sup>. Notably, however, the broad feature in the region between 3400 cm<sup>-1</sup> and 2500 cm<sup>-1</sup>, associated with interlayer NaOH species [50], is absent, confirming that Zn(NO<sub>3</sub>)<sub>2</sub> treatment results in the full exchange and removal of any Na<sup>+</sup> species from magadiite throughout the bulk of the magadiite silicate. Another remarkable feature of the infrared spectrum of magadiite after Zn  $(NO_3)_2$  treatment is the absence of bands that indicate the presence of nitrate groups in the region at  $\sim 1350 \, \text{cm}^{-1}$  (Fig. 6c; for a reference FTIR spectrum of Zn(OH)(NO<sub>3</sub>) see Supporting Information Fig. S7) [47]. Altogether, these data show that (i) the structure of magadiite layers does not change upon treatment with Zn(NO<sub>3</sub>)<sub>2</sub>, (ii) Zn<sup>2+</sup> cations intercalate and replace all interlayer Na+ cations, and (iii) the zinc colloids that are visible in TEM images do not contain NO<sub>3</sub><sup>-</sup> anions.

Next, in order to assess the accessibility of surface SiOH groups of magadiite before and after Zn-treatment, we use deuteration, a

commonly used method for this purpose, as the exchange of D $^+$  in D $_2$ O for H $^+$  in surface OH groups occurs readily and can be monitored by infrared spectroscopy [51]. Top infrared spectra in Fig. 6 show the effects of *in situ* D $_2$ O treatment on the respective magadiite samples. For magadiite in Fig. 6a, deuteration shifts all infrared bands to lower frequencies, with the expected  $^{\nu_{OH}}/_{\nu_{OD}}=1.35$  [54], indicating quantitative exchange of D for H. A faint feature remains non-exchanged at  $\sim 3620~{\rm cm}^{-1}$ , presumably due to a small number of silanols inaccessible in cages within defective magadiite layers.

This full accessibility of OH groups to D2O in magadiite is in stark contrast to the behaviour observed for magadiite after treatment with Zn(NO<sub>3</sub>)<sub>2</sub> (top spectrum in Fig. 6b). Upon deuteration of the Zn(NO<sub>3</sub>)<sub>2</sub>treated magadiite, features in the OD stretching region appear in the same frequency range as observed for magadiite, indicating exchange of H<sup>+</sup> for D<sup>+</sup> in this sample. However, significant intensity remains in the OH region (3000–3700 cm<sup>-1</sup>), demonstrating that a significant fraction of OH species are not being deuterated and must be inaccessible to D<sub>2</sub>O. This lack of accessibility of D2O to OH in the material treated with Zn (NO<sub>3</sub>)<sub>2</sub> is in direct contrast to the full accessibility observed for magadiite before treatment with Zn(NO<sub>3</sub>)<sub>2</sub>. This further suggests that some regions of the silicate surface of the magadiite layer after Zn treatment are now blocked and inaccessible. These inaccessible regions are located between silicate layers, because free terminal silanols with stretching vibrations at 3741 cm<sup>-1</sup>, which are located at the external surface, fully exchange with D<sub>2</sub>O in the Zn-treated material, with a the expected  $v_{OH}|_{v_{OD}}=1.35$ . This is fully consistent with the intercalation of Zn<sup>2+</sup> and growth of ZnO<sub>x</sub>(OH)<sub>y</sub> particles (vide infra), which may partially block regions of inter-layer space. We can exclude the presence of Zn-bound OH groups in Zn(NO<sub>3</sub>)<sub>2</sub>-treated magadiite, as Zn(OH) groups are fully condensed at a temperature of 200 °C - the temperature at which FTIR spectra were recorded [47].

The blockage observed upon  $D_2O$  treatment of  $Zn^{2+}$ -treated magadiite is consistent with the difference observed in external surface area increase when magadiite is treated with  $Zn^{2+}$  (40% additional surface area) and when it is  $Zn^{2+}$  treated and subsequently acid-washed (150% additional surface area).  $Zn(O)_x(OH)_y$  colloidal particles presumably block pore entrances in magadiite and prevent both  $D_2O$  access (observed lack of OH-OD exchange via infrared spectroscopy) and  $N_2$  access (only 40% external surface area measured via  $N_2$ -physisorption compared to 150% when  $Zn(O)_x(OH)_y$  is removed). Acid-washing dissolves  $Zn(O)_x(OH)_y$  particles and renders the previously blocked external surface area accessible.

#### 4.3. Effect of ball-milling on magadiite and its treatment with Zn(NO<sub>3</sub>)<sub>2</sub>

To further test our hypothesis that a growth of nanosized Zn  $(O)_x(OH)_y$  colloids on the magadiite grain boundaries causes separation and delamination of the magadiite sheets, we attempted to increase the accessibility of existing grain boundaries as well as create new ones via ball milling (i.e. mechanically mixing magadiite in a planetary mill). If our hypothesis is correct, then these two effects will allow for additional sheet separation and for additional creation of external surface area during Zn treatment, though other effects could also be at play, such as increased reactive surface area due to sheet breakage also facilitating delamination, separate from this hypothesis.

We first characterized ball-milled magadiite to determine possible effects of ball-milling on its textural properties. The same positions of the peaks as well as their relative intensities in the X-ray diffraction data of Fig. 3 demonstrates that ball-milling had little effect on the structure of magadiite. However, for ball-milled magadiite, non-basal reflection intensities in the 2theta range of 25°–30° are slightly lower than those of as-made magadiite (see Fig. S5), which indicates that intra-layer long-range order decreases during ball-milling, in line with observed TEM images (Fig. 5) that show "sheet breaking", which we surmise occurs along with creation of new grain-boundaries within layers. N<sub>2</sub> physisorption data in Fig. 4 and Figs. S1 and S2 (Supporting

Information) show an external surface area of 11 m²/g for ball-milled magadiite, which is similar to the external surface area measured for magadiite prior to ball milling. Consistent with the small differences between magadiite before and after ball milling, TEM and HAADF-STEM images in Fig. 5 show similarity in that both samples consist of a layered structure, with TEM images of ball-milled magadiite showing clear signs of sheet-breaking. In summary, ball-milling does not significantly affect external surface area (i.e. does not delaminate magadiite on its own) and does not affect long-range order, as measured by physisorption and PXRD, respectively; however, it does lead to a slightly decrease of the crystallite (or particle) size, as measured via transmission electron microscopy in Fig. 5.

Next, in order to delaminate the ball-milled magadiite, we treated it with Zn(NO<sub>3</sub>)<sub>2</sub> solution in the same fashion as above. PXRD data in Fig. 3 show a similar change of XRD pattern after Zn(NO<sub>3</sub>)<sub>2</sub> treatment as reported above for magadiite without ball milling. The peak at 5.67° shifted to 6.38° and became broader and lower in intensity, showing loss of long-range order along the stacking direction of the layers. The amount of zinc incorporated in the ball milled sample is 4.72 wt%, which is lower than that of the zinc-treated magadiite without ballmilling (5.99 wt % Zn). This result can be interpreted on the basis of confinement-induced precipitation, which could dramatically reduce the precipitation of salt (in our case a Zn(O)x(OH)v species) in less confined spaces, after ball milling [48]. Physisorption data show an external surface area of 23 m<sup>2</sup>/g, corresponding to an external surface area increase of 109%, relative to the ball milled calcined magadiite without Zn(NO<sub>3</sub>)<sub>2</sub> treatment. TEM and HAADF-STEM images show that magadiite, after ball-milling and Zn(NO<sub>3</sub>)<sub>2</sub> treatment, is significantly different from the ball-milled magadiite shown in Fig. 5. The Zn-treated material in Fig. 5 shows disordered arrangements of magadiite layers with signs of delamination. Additional HAADF-STEM images of ballmilled and Zn<sup>2+</sup>-treated magadiite shown in Fig. S3 also show the presence of nanoparticles, which have a distinctly different appearance than that of magadiite. These particles presumably consist of Zn (O)<sub>x</sub>(OH)<sub>v</sub> colloids.

Next, we acid-washed the magadiite that was ball-milled prior to Zn treatment. The resulting material showed an increase of external surface area to 31 m<sup>2</sup>/g from 23 m<sup>2</sup>/g before acid washing, corresponding to a total external surface area increase of 182%, relative to the ballmilled and calcined magadiite without Zn(NO<sub>3</sub>)<sub>2</sub> treatment and acid washing (11 m<sup>2</sup>/g). This increase in surface area is also reflected in HAADF-STEM images shown in Fig. 5, which show mostly delaminated layers after acid-washing, similar in nanoscale morphology to delaminated layers in the material without prior ball milling. Altogether, these data show that Zn-treatment of ball-milled magadiite followed by acidwashing creates a delaminated material with increased external surface area. However, in stark contrast to Zn-treated magadiite without ballmilling, which underwent delamination according to HAADF-STEM only after acid-washing, not after Zn-treatment alone, the delaminated nature of ball-milled magadiite is already visible in HAADF-STEM images after Zn-treatment, prior to acid-washing (corresponding to material E in Fig. 2).

### 4.4. A comparison of the effect of Zn-treatment and acid-washing on magadiite and ball-milled magadiite

 ${\rm Zn}^{2+}$  treatment of magadiite creates 40% additional external surface area, while  ${\rm Zn}^{2+}$  treatment of ball-milled magadiite creates 109% additional external surface area. The increased change in relative external surface area for the sample that underwent ball milling can be explained as follows: ball milling may either create new grain boundaries within the magadiite or it may increase the accessibility of existing grain boundaries, or possibly both. The former involves the creation of new grain boundaries that  ${\rm Zn}({\rm O})_x({\rm OH})_y$  can penetrate and wedge apart magadiite layers from. The latter involves a greater degree of magadiite-layer separation, even in the presence of  ${\rm Zn}({\rm O})_x({\rm OH})_y$  colloids

(i.e., before Zn removal via acid washing).

To investigate the possibility of ball-milling creating new grain boundaries, we examine the increase in external surface area following acid washing (i.e.  $\mathrm{Zn(O)_x(OH)_y}$  colloid removal).  $\mathrm{Zn^{2+}}$  treatment and acid washing of magadiite leads to an increase in external surface area of 150% for magadiite and 182% for ball-milled magadiite. If ball milling did not synthesize new grain boundaries, our expectation would be that after Zn treatment and acid washing, both materials would be delaminated to the same extent This is because a combination of Zn treatment and acid washing would be expected to equally delaminate all grain boundaries in magadiite that are present prior to ball milling. Therefore, based on the greater increase in surface area after acid washing for the ball-milled sample (182% vs 150% for non-ball-milled sample), we conclude that ball milling modestly increases the number of grain boundaries. The extent of grain-boundary increase between the two samples would be estimated at (182–150)/150 = 21%.

Next, we examine evidence related to whether ball milling increases the accessibility of existing grain boundaries, by comparing the external surface areas of magadiite and ball-milled magadiite after Zn2+ treatment, prior to acid washing. Zn<sup>2+</sup> treatment of magadite creates 40% additional external surface area, while Zn2+ treatment of ball-milled magadiite creates 109% additional external surface area. In principle, the difference in magnitude between these two numbers - spanning a factor of 2.7-fold - could be the result of ball milling either increasing the accessibility of existing grain boundaries or creating new accessible grain boundaries. However, the extent to which ball milling creates new grain boundaries is modest (21%, vide supra) and smaller than the difference between 109% and 40%, for the two comparative samples before acid washing. We therefore infer that the major role of ball milling is to increase accessibility of existing grain boundaries rather than to create new ones. Part of this enhanced accessibility could include sheet breakage.

These roles of ball milling are reflected schematically in Fig. 2. Zn<sup>2+</sup> treatment of magadiite prior to ball milling results in Zn(O)<sub>v</sub>(OH)<sub>v</sub> colloid infiltration but only a small increase in external surface area prior to acid washing. Inaccessibility of surface area after Zn treatment, detected by FTIR spectroscopy and N2 physisorption, indeed suggests that Zn(O)<sub>x</sub>(OH)<sub>y</sub> colloidal particles block access to the newly created external surface area within the narrow grain boundaries. TEM and HAADF-STEM images in Fig. 5 support this, as these images show that the Zn<sup>2+</sup>-treated magadiite appears to be intact but separated by darks spots, presumably Zn(O)x(OH)v colloids. In contrast, the more accessible grain boundaries in ball-milled magadiite, Zn<sup>2+</sup> treatment allow the growth of larger Zn(O)<sub>x</sub>(OH)<sub>v</sub> colloids that act efficiently as wedges to separate layers, consistent with TEM and HAADF-STEM data in Fig. 5 and Fig. S2, which show the delaminated nature of ball-milled and  $Zn^{2+}$ -treated magadiite as well as presence of  $Zn(O)_x(OH)_y$  colloids; the latter are now large enough to be visualized for the sample after ball milling.

#### 5. Conclusion

 $\rm Zn(NO_3)_2$  treatment delaminates both magadiite and ball-milled magadiite, resulting in 150% and 182% more external surface area relative to magadiite, respectively, after acid washing. An analysis of extent of external surface synthesized relative to magadiite points to the following effects of ball milling on magadiite delamination:

- Ball milling creates some new grain boundaries, which result in the enhanced external surface area of the ball-milled versus the nonball-milled sample after Zn<sup>2+</sup>-treatment followed by acid washing.
- Ball milling of magadiite leads to a more open structure of existing grain boundaries, resulting in a greater relative increase in external surface area of magadiite after Zn(NO<sub>3</sub>)<sub>2</sub> treatment.

All of these conclusions point to a mechanism of Zn<sup>2+</sup>-facilitated

magadiite delamination, which may involve  $Zn(O)_x(OH)_y$  colloids nucleating and growing in grain boundaries of the magadiite material, where they act as wedges to force magadiite layers apart, as shown in Fig. 2. The percentage of increase in external surface area resulting from delamination of magadiite silicate followed by acid-washing (150%) is comparable to that for the borosilicate DZ-1 (147%), made from layered zeolite precursor ERB-1(P), via a similar delamination procedure, involving simultaneous  $Zn(NO_3)_2$  and  $HNO_3$  acid treatment [33]. These data from magadiite delamination may shed light on the role of  $Zn^{2+}$  in zeolite delamination via  $Zn^{2+}$  treatment, which could also proceed through formation of  $Zn(O)_x(OH)_y$  colloids, which nucleate and grow in grain boundaries of the borosilicate zeolites.

#### Conflicts of interest

The authors declare the following competing financial interest(s): (1) The funding for the research partially came from Chevron Energy Technology Co. and (2) Stacey I. Zones is an employee and stockholder in Chevron Corp.

#### Acknowledgements

The authors are grateful to the Management and Transfer of Hydrogen via Catalysis Program funded by Chevron Corporation and the National Science Foundation (PFI:AIR-TT 1542974) for the synthesis of materials, and the Office of Basic Energy Sciences of Department of Energy (DE-FG02-05ER15696) for materials characterization. Work at the Molecular Foundry was supported by the Office of Science, Office of Basic Energy Sciences, of the U.S. Department of Energy under Contract No. DE-AC02-05CH11231. C.S. acknowledges Deutsche Forschungsgemeinschaft (DFG) for a research fellowship.

#### Appendix A. Supplementary data

Supplementary data to this article can be found online at https://doi.org/10.1016/j.micromeso.2019.03.048.

#### References

- W.J. Roth, MCM-22 zeolite family and the delaminated zeolite MCM-56 obtained in one-step synthesis, Stud. Surf. Sci. Catal, 2005, pp. 19–26, https://doi.org/10. 1016/S0167-299105380317-9
- [2] W.J. Roth, Chapter 7 Synthesis of delaminated and pillared zeolitic materials, Stud. Surf. Sci. Catal. 168 (2007) 221–239, https://doi.org/10.1016/S0167-2991(07) 80795-6.
- [3] W.J. Roth, D.L. Dorset, Expanded view of zeolite structures and their variability based on layered nature of 3-D frameworks, Microporous Mesoporous Mater. 142 (2011) 32–36, https://doi.org/10.1016/j.micromeso.2010.11.007.
- [4] W.J. Roth, D.L. Dorset, G.J. Kennedy, Discovery of new MWW family zeolite EMM-10: identification of EMM-10P as the missing MWW precursor with disordered layers, Microporous Mesoporous Mater. 142 (2011) 168–177, https://doi.org/10.1016/j.micromeso.2010.10.052.
- [5] P. Eliášová, M. Opanasenko, P.S. Wheatley, M. Shamzhy, M. Mazur, P. Nachtigall, W.J. Roth, R.E. Morris, J. Čejka, The ADOR mechanism for the synthesis of new zeolites, Chem. Soc. Rev. 44 (2015) 7177–7206, https://doi.org/10.1039/ c5cs00045a.
- [6] M.V. Opanasenko, W.J. Roth, J. Čejka, Two-dimensional zeolites in catalysis: current status and perspectives, Catal. Sci. Technol. 6 (2016) 2467–2484, https://doi.org/10.1039/c5cv02079d.
- [7] K. Verguts, J. Coroa, C. Huyghebaert, S. De Gendt, S. Brems, Graphene delamination using "electrochemical methods": an ion intercalation effect, Nanoscale 10 (2018) 5515–5521, https://doi.org/10.1039/c8nr00335a.
- [8] K. Suzuki, Preparation of delaminated clay having a narrow micropore distribution in the presence of hydroxyaluminum cations and polyvinyl alcohol, Clay Clay Miner. 36 (1988) 147–152, https://doi.org/10.1346/CCMN.1988.0360208.
- [9] I. Ogino, E.A. Eilertsen, S.J. Hwang, T. Rea, D. Xie, X. Ouyang, S.I. Zones, A. Katz, Heteroatom-tolerant delamination of layered zeolite precursor materials, Chem. Mater. 25 (2013) 1502–1509, https://doi.org/10.1021/cm3032785.
- [10] A. Okrut, M. Aigner, C. Schöttle, N.A. Grosso-Giordano, S.J. Hwang, X. Ouyang, S. Zones, A. Katz, SSZ-70 borosilicate delamination without sonication: effect of framework topology on olefin epoxidation catalysis, Dalton Trans. 47 (2018) 15082–15090, https://doi.org/10.1039/C8DT03044H.
- [11] X. Ouyang, S.J. Hwang, R.C. Runnebaum, D. Xie, Y.J. Wanglee, T. Rea, S.I. Zones, A. Katz, Single-step delamination of a MWW borosilicate layered zeolite precursor

- under mild conditions without surfactant and sonication, J. Am. Chem. Soc. 136 (2014) 1449–1461, https://doi.org/10.1021/ja410141u.
- [12] B. Xie, D. De Vos, H. Gies, X. Bao, F.-S. Xiao, B. Yilmaz, A. Grünewald-Lüke, H. Imai, W. Zhang, T. Tatsumi, U. Müller, Layered precursors for new zeolitic materials: synthesis and characterization of B-RUB-39 and its condensation product B-RUB-41, Microporous Mesoporous Mater. 147 (2011) 102–109, https://doi.org/10.1016/j.micromeso.2011.05.036.
- [13] W.J. Roth, J. Čejka, Two-dimensional zeolites: dream or reality? Catal. Sci. Technol. 1 (2011) 43, https://doi.org/10.1039/c0cy00027b.
- [14] A. Corma, V. Fornes, S.B. Pergher, T.L.M. Maesen, J.G. Buglass, Delaminated zeolite precursors as selective acidic catalysts, Nature 396 (1998) 353–356, https://doi. org/10.1038/24592.
- [15] S. Maheshwari, E. Jordan, S. Kumar, F.S. Bates, R.L. Penn, D.F. Shantz, M. Tsapatsis, Layer structure preservation during swelling, pillaring, and exfoliation of a zeolite precursor, J. Am. Chem. Soc. 130 (2008) 1507–1516, https://doi.org/10.1021/ ja0777711i.
- [16] S. Maheshwari, C. Martínez, M. Teresa Portilla, F.J. Llopis, A. Corma, M. Tsapatsis, Influence of layer structure preservation on the catalytic properties of the pillared zeolite MCM-36, J. Catal. 272 (2010) 298–308, https://doi.org/10.1016/j.jcat. 2010.04.011
- [17] I. Ogino, M.M. Nigra, S.J. Hwang, J.M. Ha, T. Rea, S.I. Zones, A. Katz, Delamination of layered zeolite precursors under mild conditions: synthesis of UCB-1 via fluoride/ chloride anion-promoted exfoliation, J. Am. Chem. Soc. 133 (2011) 3288–3291, https://doi.org/10.1021/ja111147z.
- [18] E.A. Eilertsen, I. Ogino, S.J. Hwang, T. Rea, S. Yeh, S.I. Zones, A. Katz, Nonaqueous fluoride/chloride anion-promoted delamination of layered zeolite precursors: synthesis and characterization of UCB-2, Chem. Mater. 23 (2011) 5404–5408, https://doi.org/10.1021/cm202364q.
- [19] J.E.F.C. Gardolinski, G. Lagaly, Grafted organic derivatives of kaolinite: II. Intercalation of primary n-alkylamines and delamination, Clay Miner. 40 (2006) 547–556, https://doi.org/10.1180/0009855054040191.
- [20] O.D. Pavel, B. Cojocaru, E. Angelescu, V.I. Pârvulescu, The activity of yttrium-modified Mg,Al hydrotalcites in the epoxidation of styrene with hydrogen peroxide, Appl. Catal. Gen. 403 (2011) 83–90, https://doi.org/10.1016/j.apcata.2011.06.
- [21] N.D. Hould, S. Kumar, M. Tsapatsis, V. Nikolakis, R.F. Lobo, Structure and colloidal stability of nanosized zeolite beta precursors, Langmuir 26 (2010) 1260–1270, https://doi.org/10.1021/la902445c.
- [22] S. Pulinthanathu Sree, J. Dendooven, P. Magusin, K. Thomas, J.-P. Gilson, F. Taulelle, C. Detavernier, J. Martens, Hydroisomerization and hydrocracking activity enhancement of hierarchical ZSM-5 zeolite catalyst via atomic layer deposition of aluminium, Catal. Sci. Technol. 6 (2016) 6177–6186, https://doi.org/10.1039/C6CY00780E.
- [23] K.-G. Haw, J.-M. Goupil, J.-P. Gilson, N. Nesterenko, D. Minoux, J.-P. Dath, V. Valtchev, Embryonic ZSM-5 zeolites: zeolitic materials with superior catalytic activity in 1,3,5-triisopropylbenzene dealkylation, New J. Chem. 40 (2016) 4307–4313, https://doi.org/10.1039/C5NJ03310A.
- [24] A.G. Machoke, İ.Y. Knoke, S. Lopez-Orozco, M. Schmiele, T. Selvam, V.R.R. Marthala, E. Spiecker, T. Unruh, M. Hartmann, W. Schwieger, Synthesis of multilamellar MFI-type zeolites under static conditions: the role of gel composition on their properties, Microporous Mesoporous Mater. 190 (2014) 324–333, https:// doi.org/10.1016/j.micromeso.2014.02.026.
- [25] M.E. Davis, The quest for extra-large pore, crystalline molecular sieves, Chem. Eur J. 3 (1997) 1745–1750, https://doi.org/10.1002/chem.19970031104.
- [26] J. Jiang, J. Yu, A. Corma, Extra-large-pore zeolites: bridging the gap between micro and mesoporous structures, Angew. Chem. Int. Ed. 49 (2010) 3120–3145, https:// doi.org/10.1002/anie.200904016.
- [27] M. Choi, K. Na, J. Kim, Y. Sakamoto, O. Terasaki, R. Ryoo, Stable single-unit-cell nanosheets of zeolite MFI as active and long-lived catalysts, Nature 461 (2009) 246–249, https://doi.org/10.1038/nature08493.
- [28] J. Přech, R.E. Morris, J. Čejka, Selective oxidation of bulky organic sulphides over layered titanosilicate catalysts, Catal. Sci. Technol. 6 (2016) 2775–2786, https:// doi.org/10.1039/C5CY02083B.
- [29] M. Mazur, P.S. Wheatley, M. Navarro, W.J. Roth, M. Položij, A. Mayoral, P. Eliášová, P. Nachtigall, J. Čejka, R.E. Morris, Synthesis of 'unfeasible' zeolites, Nat. Chem. 8 (2015) 58–62, https://doi.org/10.1038/nchem.2374.
- [30] W. Fan, M.A. Snyder, S. Kumar, P.-S. Lee, W.C. Yoo, A.V. McCormick, R.L. Penn, A. Stein, M. Tsapatsis, Hierarchical nanofabrication of microporous crystals with ordered mesoporosity, Nat. Mater. 7 (2008) 984–991, https://doi.org/10.1038/ nmat2302.
- [31] K. Na, C. Jo, J. Kim, K. Cho, J. Jung, Y. Seo, R.J. Messinger, B.F. Chmelka, R. Ryoo, Directing zeolite structures into hierarchically nanoporous architectures, Science 333 (80) (2011) 328–332, https://doi.org/10.1126/science.1204452.
- [32] X. Zhang, D. Liu, D. Xu, S. Asahina, K.A. Cychosz, K.V. Agrawal, Y. Al Wahedi,

- A. Bhan, S. Al Hashimi, O. Terasaki, M. Thommes, M. Tsapatsis, Synthesis of self-pillared zeolite nanosheets by repetitive branching, Science 336 (80) (2012) 1684–1687, https://doi.org/10.1126/science.1221111.
- [33] X. Ouyang, Y.-J. Wanglee, S.-J. Hwang, D. Xie, T. Rea, S.I. Zones, A. Katz, Novel surfactant-free route to delaminated all-silica and titanosilicate zeolites derived from a layered borosilicate MWW precursor, Dalton Trans. 43 (2014) 10417–10429, https://doi.org/10.1039/c4dt00383g.
- [34] A. Inayat, C. Schneider, W. Schwieger, Organic-free synthesis of layer-like FAU-type zeolites, Chem. Commun. 51 (2015) 279–281, https://doi.org/10.1039/ C4CC07947G
- [35] X. Ouyang, S.J. Hwang, D. Xie, T. Rea, S.I. Zones, A. Katz, Heteroatom-substituted delaminated zeolites as solid lewis acid catalysts, ACS Catal. 5 (2015) 3108–3119, https://doi.org/10.1021/cs5020546.
- [36] B. Marler, H. Gies, Hydrous layer silicates as precursors for zeolites obtained through topotactic condensation: a review, Eur. J. Mineral. 24 (2012) 405–428, https://doi.org/10.1127/0935-1221/2012/0024-2187.
- [37] J.M. Garcés, Hypothetical structures of magadiite and sodium octosilicate and structural relationships between the layered alkali metal silicates and the mordenite- and pentasil-group Zeolites1, Clay Clay Miner. 36 (1988) 409–418, https:// doi.org/10.1346/CCMN.1988.0360505.
- [38] S. Li, Y. Mao, H.J. Ploehn, Interlayer functionalization of magadiite with sulfurcontaining organosilanes, Colloids Surfaces A Physicochem. Eng. Asp. 506 (2016) 320–330, https://doi.org/10.1016/j.colsurfa.2016.06.043.
- [39] G. Lagaly, K. Beneke, Magadiite and H-Magadiite: I. Sodium magadiite and some of its derivatives, Am. Mineral. 60 (1975) 642–649.
- [40] B. Zebib, J.-F. Lambert, J. Blanchard, M. Breysse, LRS-1, a new mesoporous material with high acidity, Chem. Mater. 18 (2006) 34–40, https://doi.org/10.1021/ cm050643j.
- [41] Y. Bi, J.-F. Lambert, Y. Millot, S. Casale, J. Blanchard, S. Zeng, H. Nie, D. Li, Relevant parameters for obtaining high-surface area materials by delamination of magadiite, a layered sodium silicate, J. Mater. Chem. 21 (2011) 18403, https://doi. org/10.1039/c1jm13108g.
- [42] K. Ozawa, Y. Nakao, Z. Cheng, D. Wang, M. Osada, R. Okada, K. Saeki, H. Itoh, F. Iso, Fabrication of novel composites of ZnO-nanoparticles and magadiite, Mater. Lett. 63 (2009) 366–369, https://doi.org/10.1016/j.matlet.2008.10.038.
- [43] Z. Qin, G. Melinte, J.P. Gilson, M. Jaber, K. Bozhilov, P. Boullay, S. Mintova, O. Ersen, V. Valtchev, The mosaic structure of zeolite crystals, Angew. Chem. Int. Ed. 55 (2016) 15049–15052, https://doi.org/10.1002/anie.201608417.
- [44] M. Moliner, J.E. Gabay, C.E. Kliewer, R.T. Carr, J. Guzman, G.L. Casty, P. Serna, A. Corma, Reversible transformation of Pt nanoparticles into single atoms inside high-silica chabazite zeolite, J. Am. Chem. Soc. 138 (2016) 15743–15750, https://doi.org/10.1021/jacs.6b10169.
- [45] M. Choi, Z. Wu, E. Iglesia, Mercaptosilane-assisted synthesis of metal clusters within zeolites and catalytic consequences of encapsulation, J. Am. Chem. Soc. 132 (2010) 9129–9137, https://doi.org/10.1021/ja102778e.
- [46] R. Marsalek, Particle size and zeta potential of ZnO, APCBEE Procedia 9 (2014) 13–17, https://doi.org/10.1016/j.apcbee.2014.01.003.
- [47] W. Stählin, H.R. Oswald, The infrared spectrum and thermal analysis of zinc hydroxide nitrate, J. Solid State Chem. 3 (1971) 252–255, https://doi.org/10.1016/0022-4596(71)90037-5.
- [48] A. Malani, K.G. Ayappa, S. Murad, Effect of confinement on the hydration and solubility of NaCl in water, Chem. Phys. Lett. 431 (2006) 88–93, https://doi.org/10. 1016/j.cplett.2006.09.071.
- [49] S.B. Badmos, A. Striolo, D.R. Cole, Aqueous hydrogen sulfide in slit-shaped silica nanopores: confinement effects on solubility, structural, and dynamical properties, J. Phys. Chem. C 122 (2018) 14744–14755, https://doi.org/10.1021/acs.jpcc. 8b04527.
- [50] J.M. Rojo, E. Ruiz-Hitzky, J. Sanz, Proton-sodium exchange in magadiite. Spectroscopic study (NMR, IR) of the evolution of interlayer OH groups, Inorg. Chem. 27 (1988) 2785–2790, https://doi.org/10.1021/ic00289a009.
- [51] E.F. Vansant, P. Van Der Voort, K.C. Vrancken, Characterization and Chemical Modification of the Silica Surface, first ed., Elsevier, 1995, https://doi.org/10. 1016/S0167-2991(06)81509-0.
- [52] P. Hoffmann, E. Knözinger, Novel aspects of mid and far IR Fourier spectroscopy applied to surface and adsorption studies on SiO2, Surf. Sci. 188 (1987) 181–198, https://doi.org/10.1016/S0039-6028(87)80150-4.
- [53] Y. Huang, Vibrational spectroscopic studies of layered silicates, Chem. Mater. 11 (1999) 1210–1217, https://doi.org/10.1021/cm980403m.
- [54] K. Chakarova, N. Drenchev, M. Mihaylov, P. Nikolov, K. Hadjiivanov, OH/OD isotopic shift factors of isolated and H-bonded surface silanol groups, J. Phys. Chem. C 117 (2013) 5242–5248, https://doi.org/10.1021/jp400106s.
- [55] P. Innocenzi, Infrared spectroscopy of sol gel derived silica-based films: a spectramicrostructure overview, J. Non-Cryst. Solids 316 (2003) 309–319.